[Supporting Information]

Thermoplasmonic Optical Fiber for Localized Neural Stimulation

*Hongki Kang[1,2,3], Woongki Hong[2], Yujin An[1], Sangjin Yoo[1,5], Hyuk-Jun Kwon[2], and Yoonkey Nam[1,4]**

[1]Department of Bio and Brain Engineering, Korea Advanced Institute of Science and Technology (KAIST), Daejeon 34141, Republic of Korea

[2]Department of Information and Communication Engineering, Daegu Gyeongbuk Institute of Science and Technology (DGIST), Daegu 42988, Republic of Korea

[3]Information & Electronics Research Institute, Korea Advanced Institute of Science and Technology (KAIST), Daejeon, Republic of Korea.

[4]KAIST Institute for Health Science and Technology, Korea Advanced Institute of Science and Technology (KAIST), Daejeon 34141, Republic of Korea.

[5]Division of Chemistry and Chemical Engineering, California Institute of Technology, Pasadena, California 91125, United States.

*Correspondence to: ynam@kaist.ac.kr

Fabrication and characterization of thermo-plasmonic optical fiber

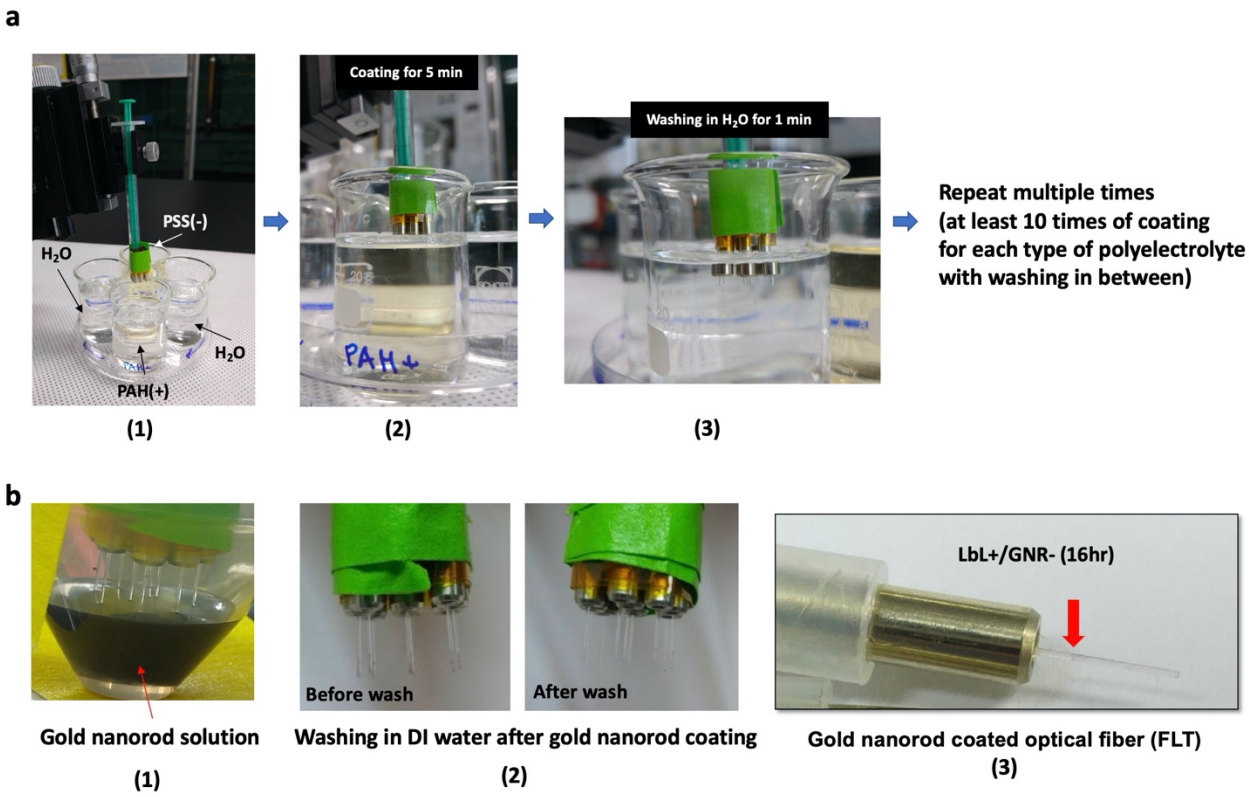

Figure S1. Optical fiber layer-by-layer polyelectrolyte coating and gold nanorod coating processes. a, Multiple optical fiber cannulas were bundled together and attached to a supporting holder (in this picture, 1 mL syringe). All of these were immersed altogether in the prepared solutions for 5 min. **b**, The LbL coated optical fiber cannulas were coated with gold nanorod in the same way of immersion. Only the tip of the optical fibers was dipped into the concentrated gold nanorod solution. After the coating, it was washed with deionized water. Despite the washing, we can confirm that the gold nanorods were strongly attached onto the surface of the optical fiber by electrostatic force (**a3**).

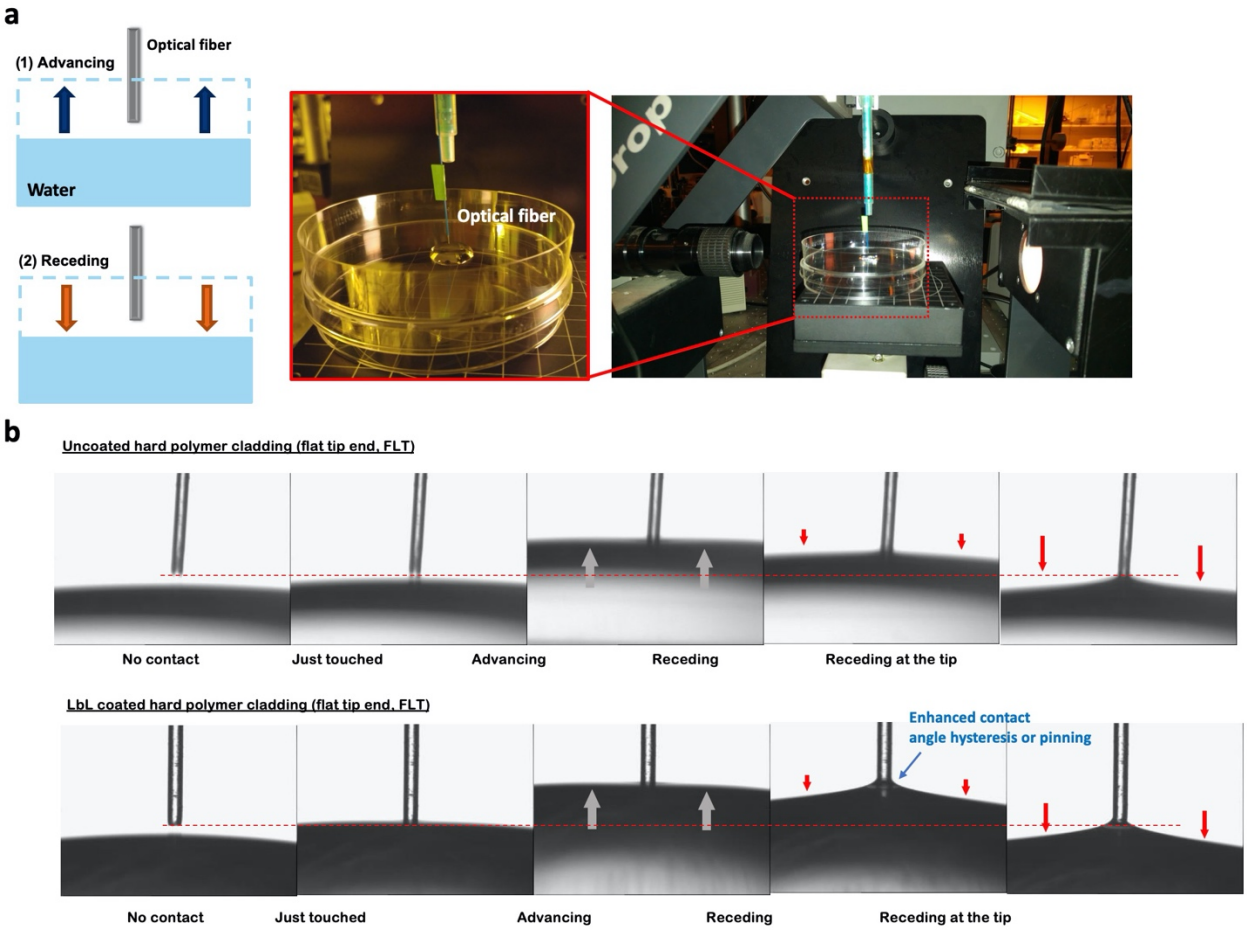

Figure S2. Surface wettability modification as a consequence of the polyelectrolyte layer-by-layer coating. a, Experimental setup and procedure of dynamic contact angle measurement. **b**, As shown in the images, LbL coated fiber showed more enhanced contact angle hysteresis (observed during receding step). It is an indication of the surface wettability change by the LbL coating.

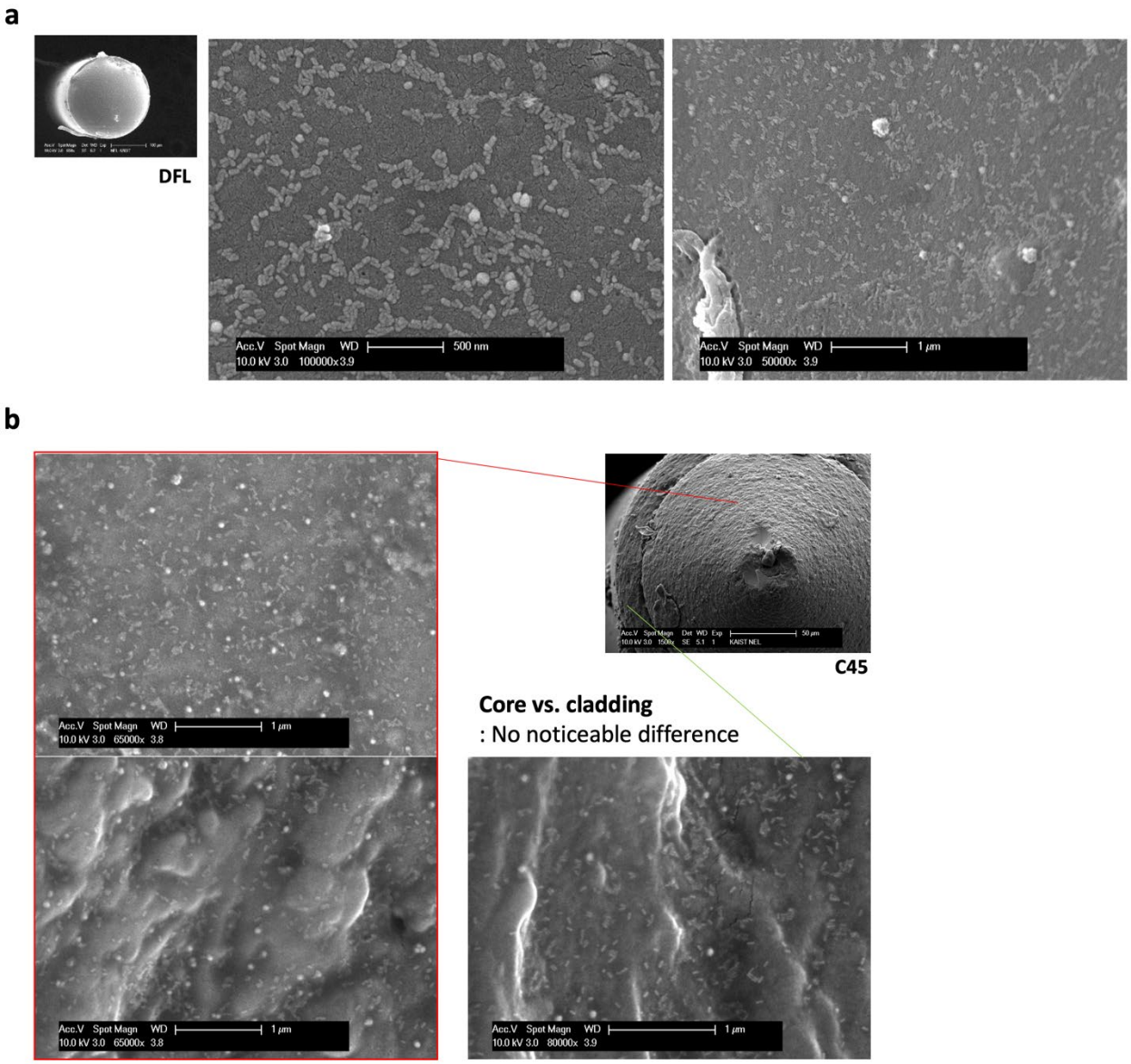

Figure S3. Scanning electron microscopy images of the surface of gold nanorod coated optical fiber cannulas. a, DFL type optical fiber core after gold nanorod coating. **b**, Gold nanorod coating on both core and cladding of the C45 type optical fiber. With the LbL coating on both core and cladding, nanorods are indeed attached on both surfaces.

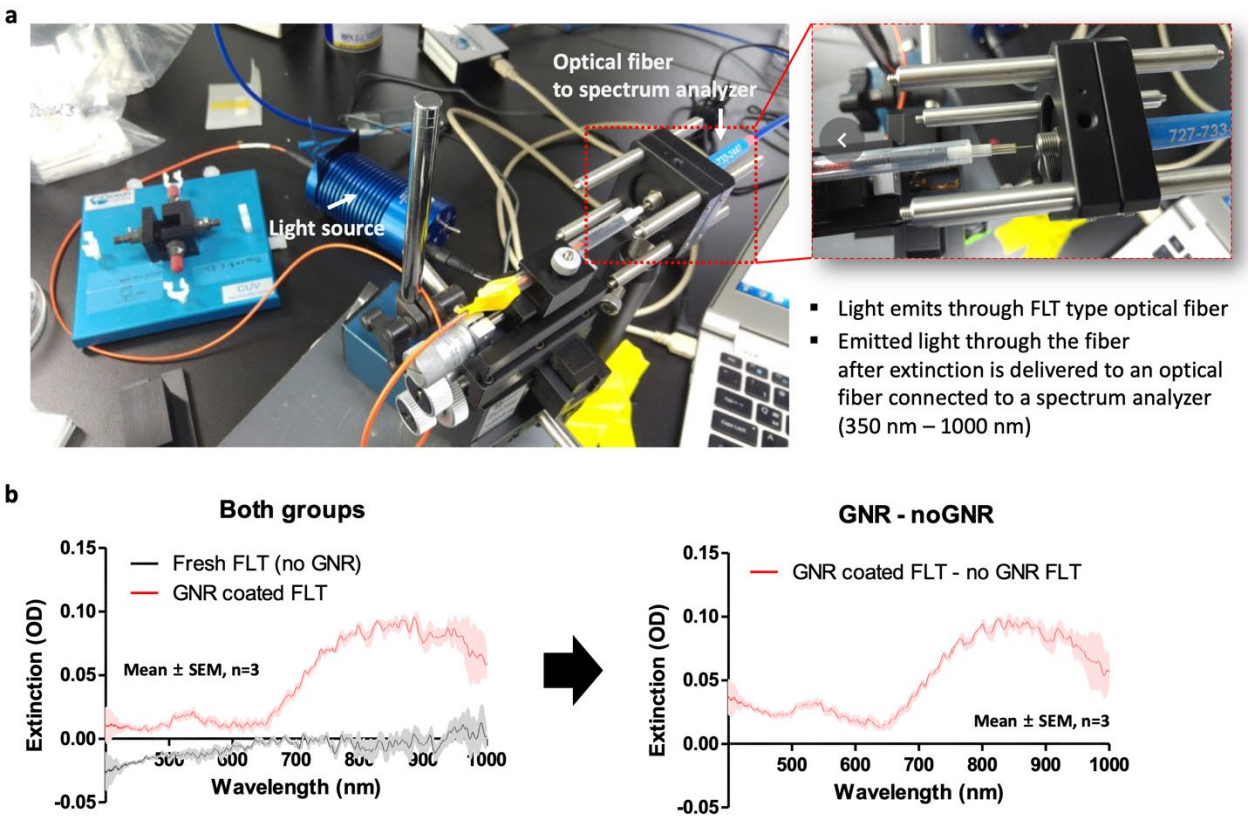

Figure S4. Extinction spectrum measurement setup. GNR coated FLT type optical fibers were used for the confirmation of wavelength selective thermo-plasmonic effect.

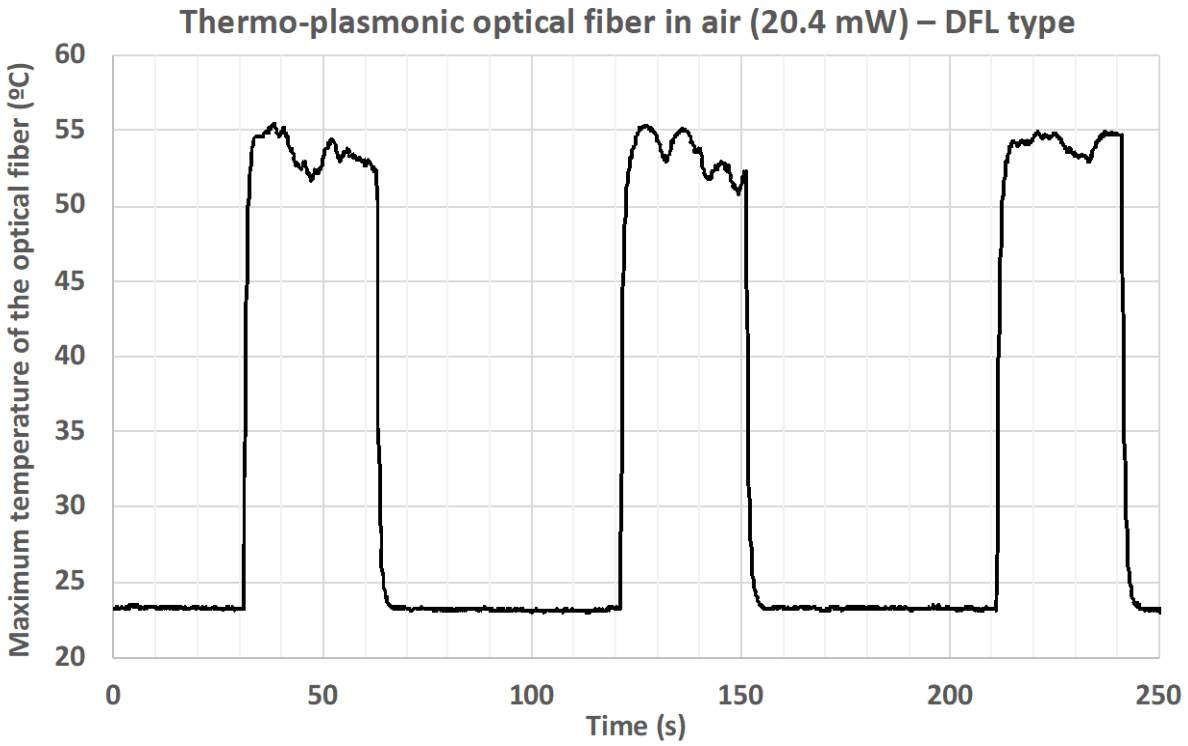

Figure S5. Photothermal effect of the TP optical fiber in air. IR camera measured the maximum temperature of the tip of the TP optical fiber placed in air with NIR laser turned on/off three times.

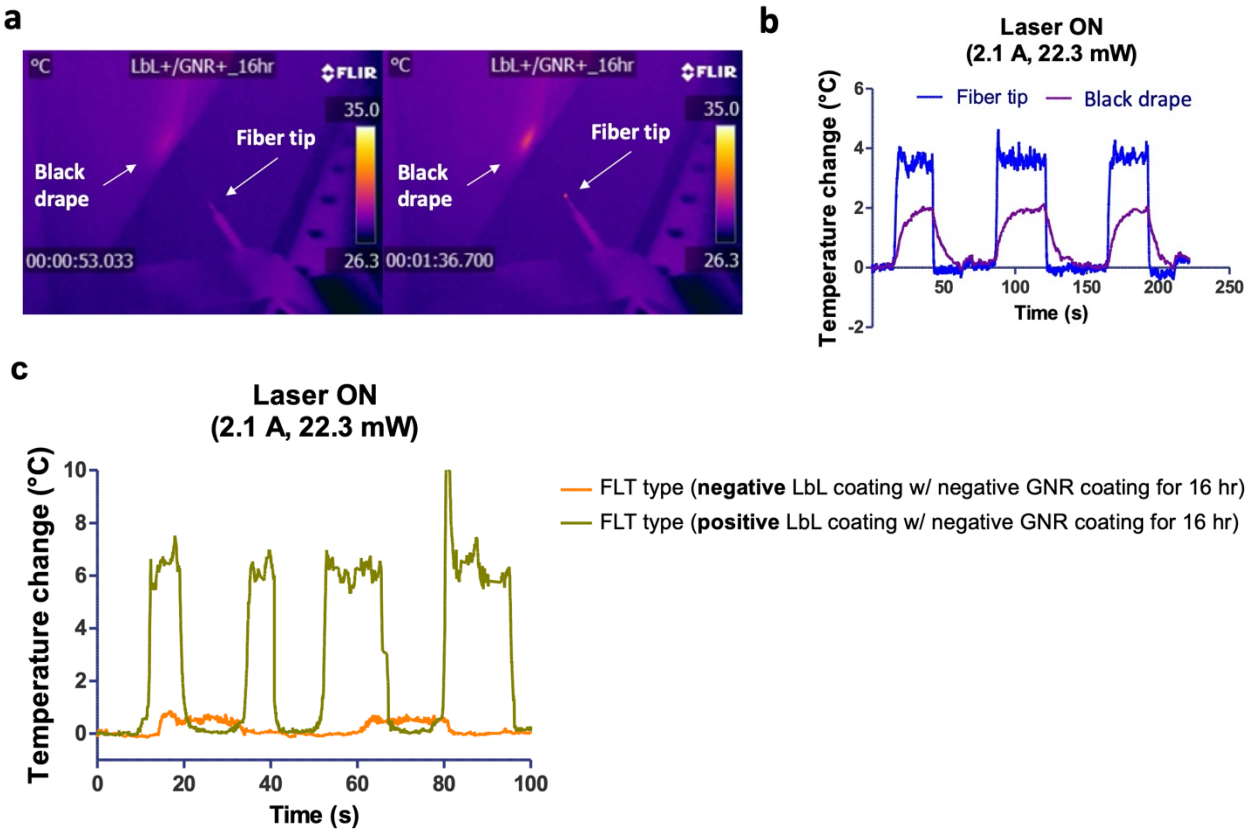

Figure S6. Thermo-plasmonic heat generation characteristics compared to non-plasmonic absorption (black drape). a, Thermographic camera measurement. During light illumination through FLT type optical fiber, both fiber tip and the nearby black drape are heated up. The optical fiber was heated up by thermo-plasmonic effect, and the black drape is by non-plasmonically. **b,** Temperature change by the thermo-plasmonic effect is much quicker than the case of non-plasmonic mechanism (black drape). **c**, Comparison of thermo-plasmonic effect in air for FLT type optical fibers with positively charged LbL coating and negatively charged LbL coating, respectively. Both fibers were coated with negatively surface charged gold nanorod for 16 hours. (Please note that the laser turn-on/off control was manual (no TTL) and power change was gradual. Maximum temperature change was observed when the 808 nm NIR laser with 22.3 mW power was delivered)

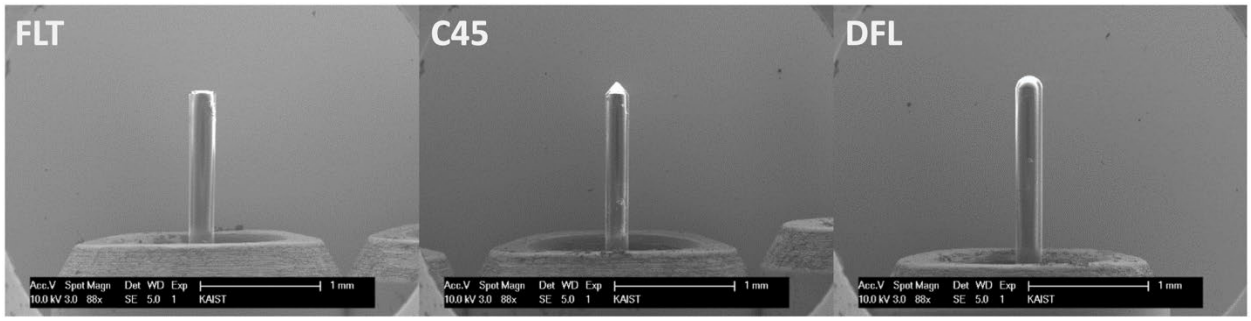

Figure S7. Scanning electron microscopy images of three different termination types of optical fibers used in this work.

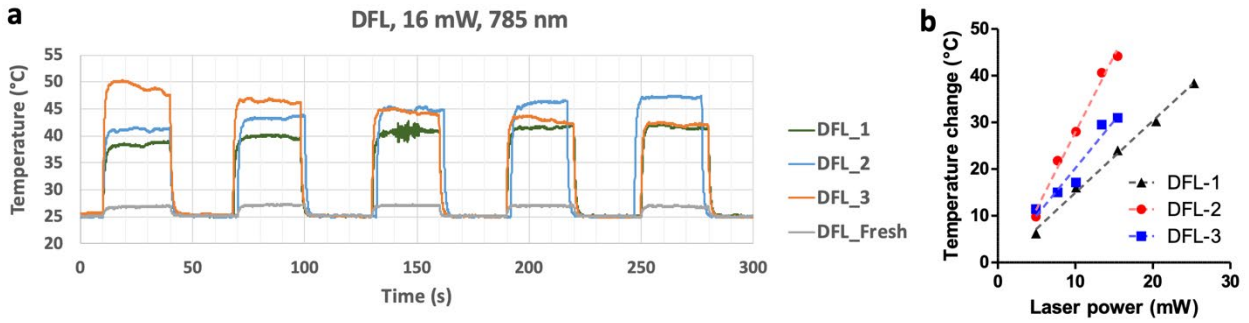

Figure S8. Thermo-plasmonic effect measurement of the DFL type optical fiber samples that were used for neural stimulation experiments. a, Temperature change upon light illumination (785 nm, 16 mW). The laser was turned on at 10 sec, and kept on for 30 sec. Then, the laser turned off for 30 sec. This process was repeated five times. **b**, Temperature change was averaged for the five trials for three different optical fiber samples which were fabricated altogether as described in **Figure S1**. The characterization in **a** was repeated for broader range of laser power, and the average data were plotted.

Photothermal stimulation on *in vitro* neuronal network

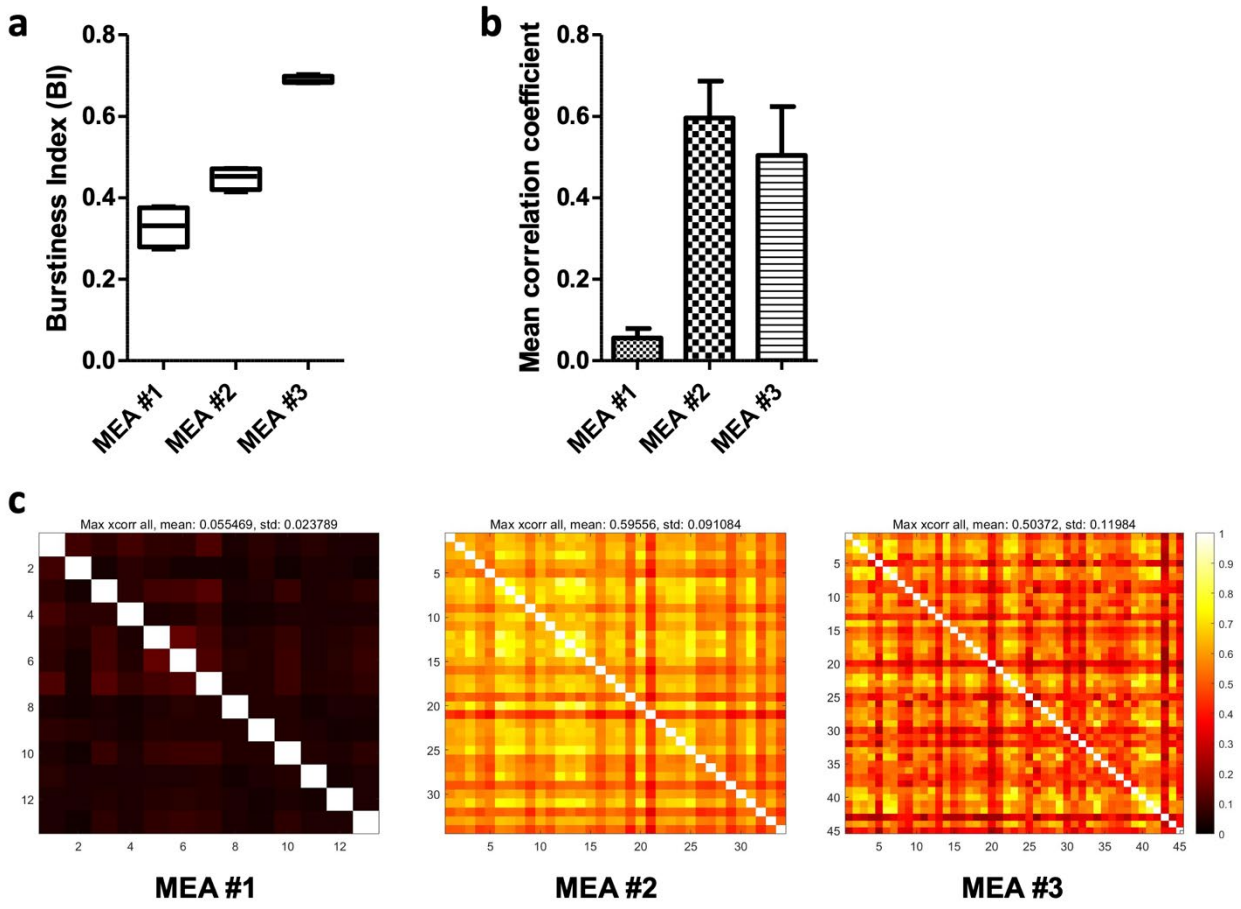

Figure S9. (a) Burstiness index of stimulated cultured neuronal network samples. Box and whiskers (minimum to maximum) (n=4 sections of baseline recordings with each section 5-minute long). (b) Mean correlation coefficient of the stimulated cultured neuronal network samples. All values represent mean ± SD (n=13, 34, 45 active channels (>0.1 spikes/sec) for MEA #1, MEA #2, MEA#3, respectively). (c) Cross-correlation matrices obtained and used for calculating the mean correlation coefficient in (b).

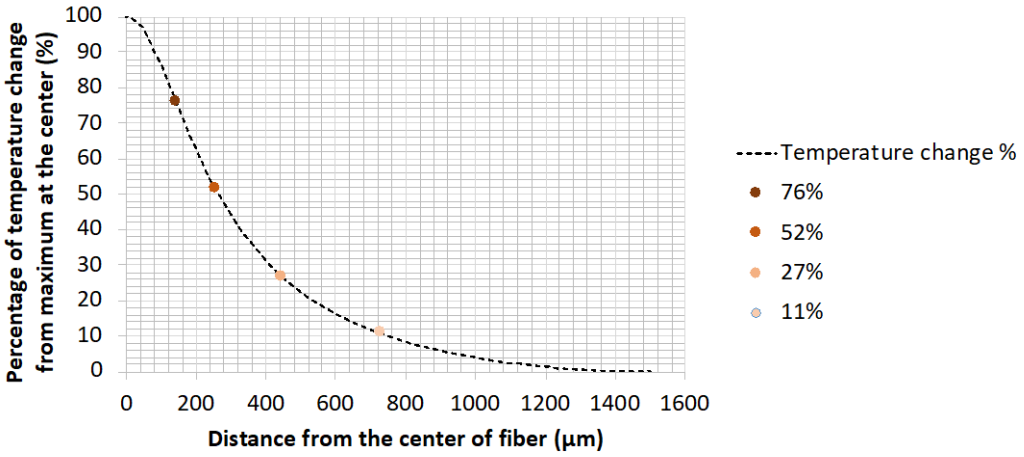

(a)

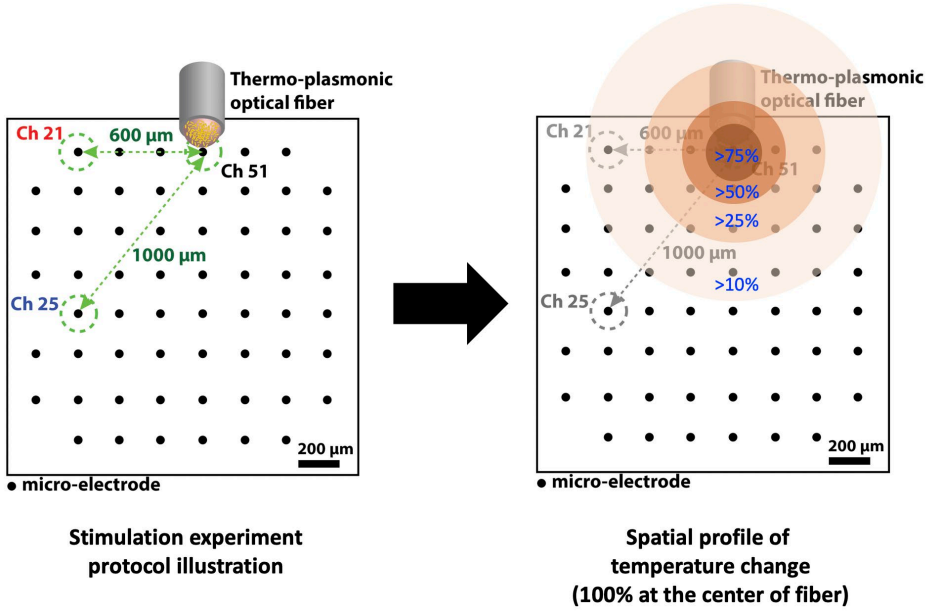

(b)

Figure S10. Computational analysis of the spatial profile of temperature change on the surface of a glass MEA. (a) Computational analysis of the spatial profile of temperature change from the center of optical fiber. The profile is drawn in 1-D, but the overall profile is concentric. (b) The spatial profile in (a) is overlaid on the experimental protocol in MEA#1 (Result 1, **Figure 3**). Concentric circles drawn around the optical fiber represent the degree of temperature change attenuation from the maximum at the center: Attenuation down to 75% at 142 µm, 50% at 253 µm, 25 % at 440 µm, and 10% at 727 µm.

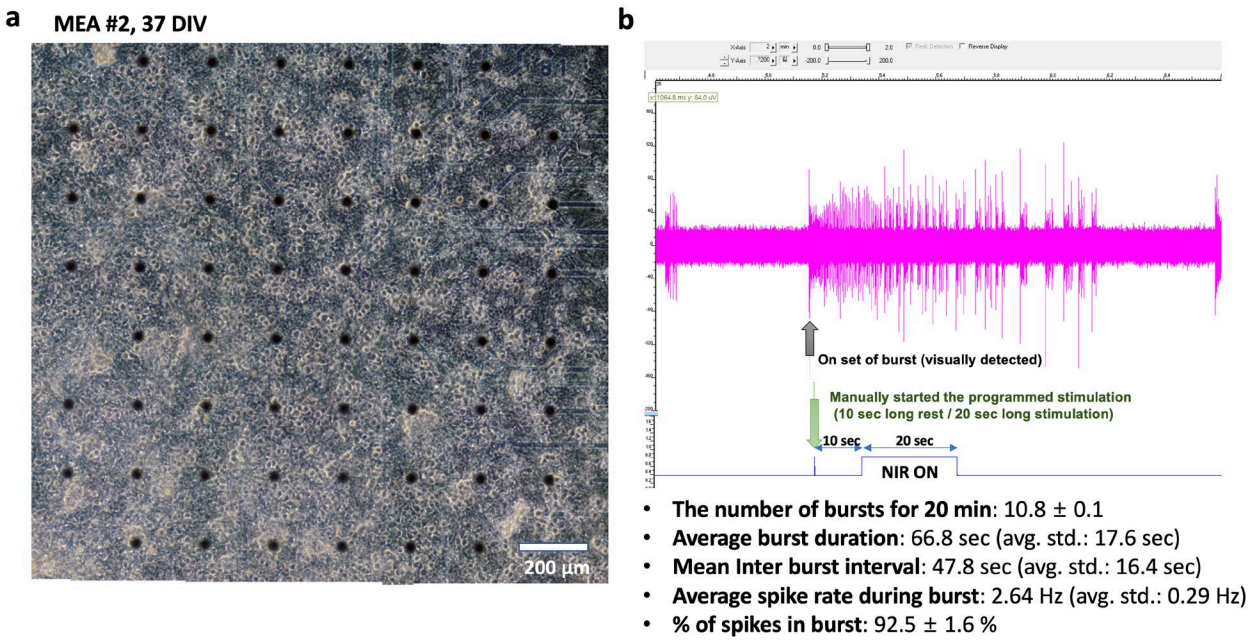

Figure S11. (MEA #2) Cultured neuronal network image, and its representative burst image with experimental procedure. a, Phase contrast image of the cultured neuronal cell on the MEA #2 at 37 DIV. **b**, This raw recording data show an exemplary burst signal from a channel and the timing of 20-sec long NIR stimulation with respect to the initial time point of the burst signal (*i.e.* approximately 10 sec delay).

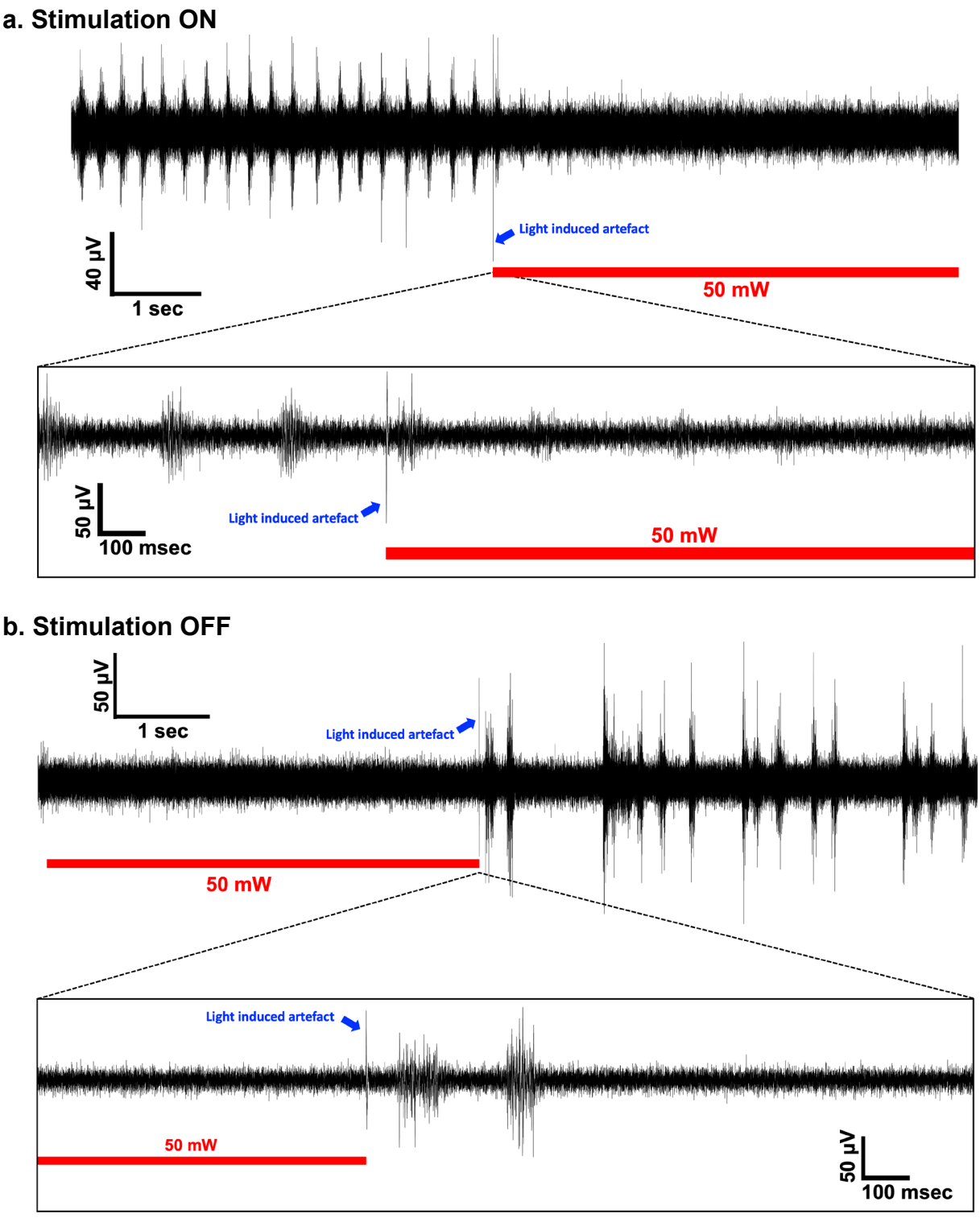

Figure S12. (MEA #2) Representative recording raw data of Ch 35 at high temporal resolution when the photothermal stimulation is on and off. Stimulation with GNR and 50 mW of near infrared laser as in Figure 4a. a, When the photothermal stimulation is turned ON. **b**, When the 20-sec long photothermal stimulation is turned OFF. Light induced artefacts are labeled in blue.

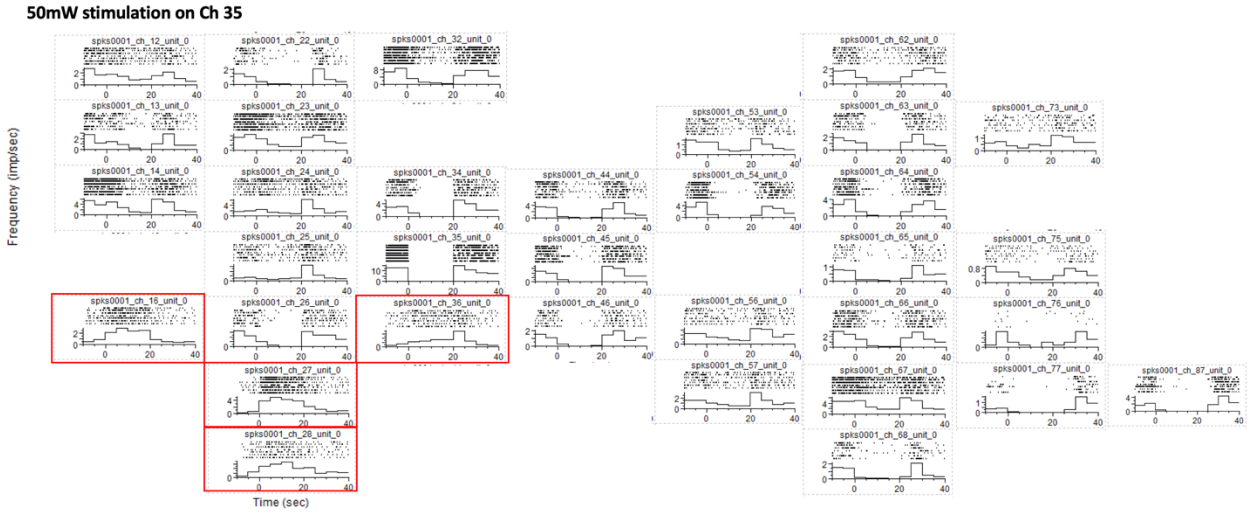

Figure S13. (MEA #2) Peri-event raster plots for all the active channels in MEA #2 upon stimulation on Ch 35. Plots for all the channels were re-organized based on the relative position of each microelectrode. Note that a few early firing channels on the left bottom are showing increased firing during the 20-sec long photothermal stimulation.

Computational analysis of the spatiotemporal temperature change during photothermal stimulation

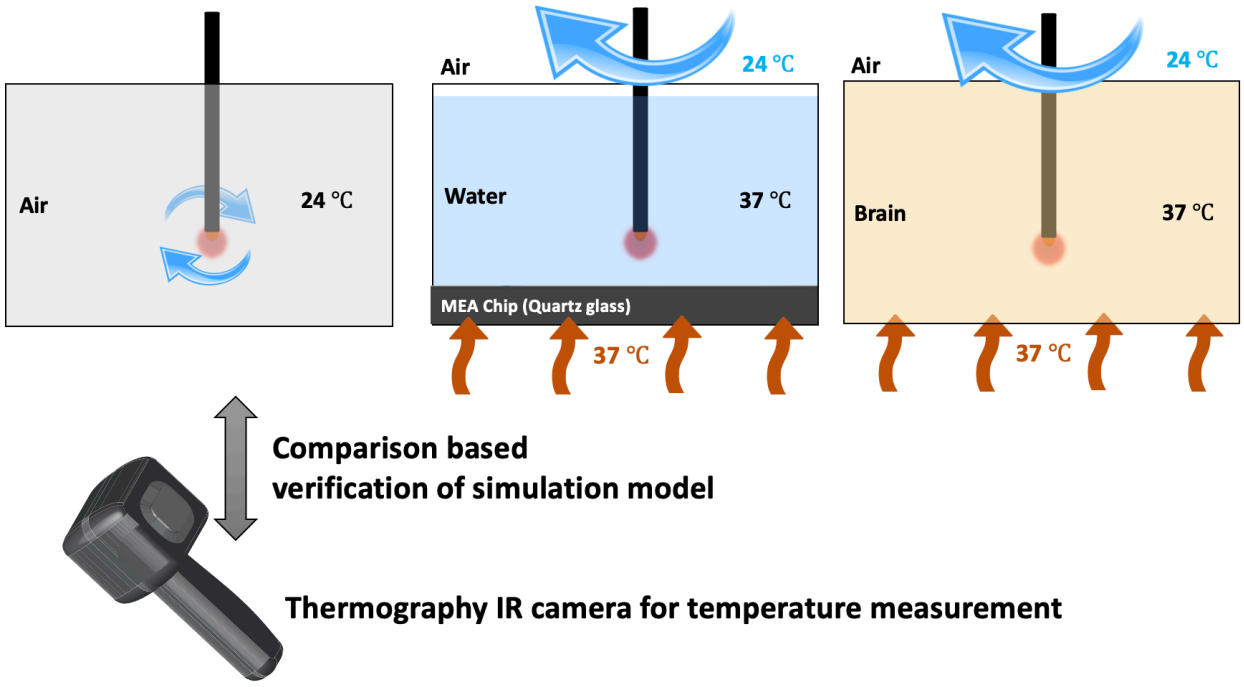

Figure S14. Computational thermal simulation conditions (environment materials, and boundary conditions). The first (from left to right) condition is when the thermo-plasmonic optical fiber is located in air. As the temperature change of the thermo-plasmonic optical fiber in air can be measured using a thermographic IR camera, the experimental measurement data were compared with the simulation in air for the verification of the simulation model. The second condition was when the thermo-plasmonic optical fiber was placed above an MEA chip, which mimics the condition of *in vitro* neural stimulation we conducted. The third simulation condition is when the optical fiber is implanted into a mouse brain. As a boundary condition, top surface was assumed to be interfacing with room temperature air with skull opened. The blue arrows represent heat convection implemented in the simulation setups.

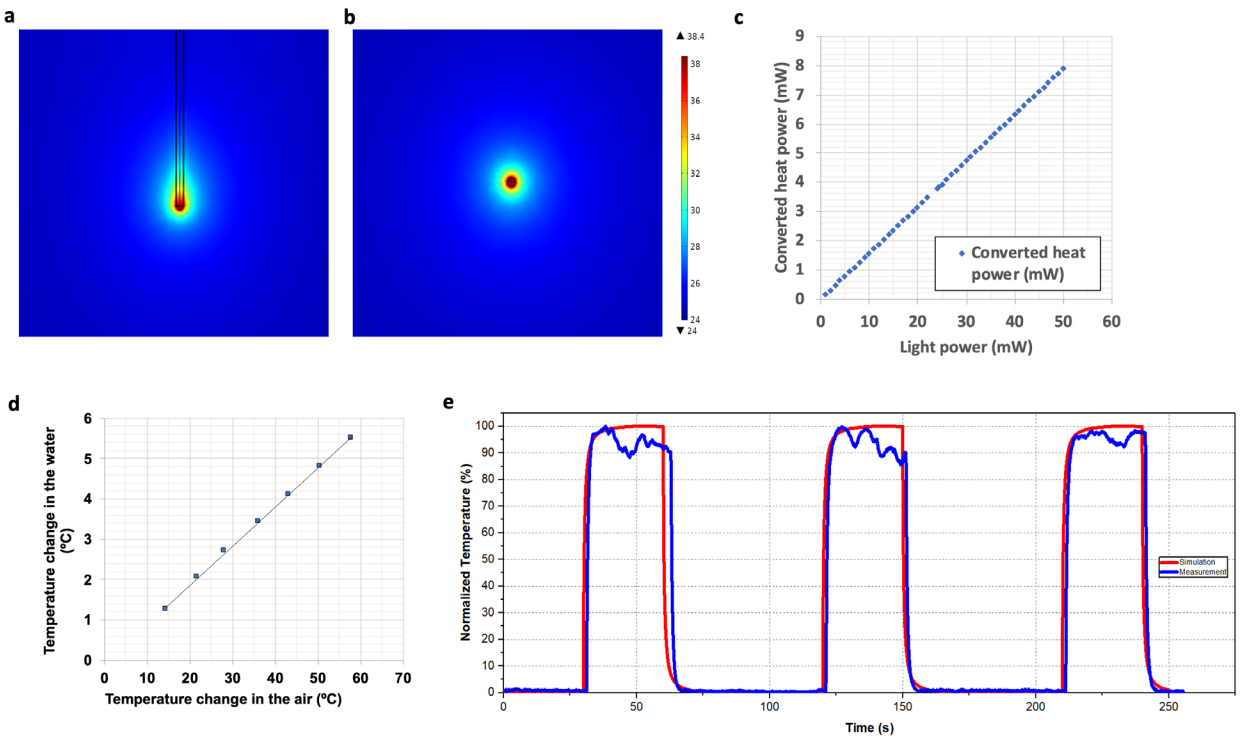

Figure S15. Computational thermal simulation of the optical fiber in air. a, Side view image of temperature change around the thermo plasmonic optical fiber placed in air with applied heat rate of 1.00 mW (equivalent to the light power of 6.71 mW). **b**, Bottom view of the same temperature change as in **a**. **c**, Calculated relationship between the converted heat rate (mW; used in simulation) and delivered light power (mW; used in the experiment). This was extracted from the comparison between simulation and experimental data described in **Figure S13**. **d**, With respect to the peak temperature change in air, y-axis value represents the peak temperature change in the *in vitro* simulation described in **Figure S13**. Significantly reduced temperature change for the same input heat rate is observed in water (*in vitro*) environment. **e**, Comparison of the simulated temperature (in air) and IR camera measured temperature change (in air) as introduced in **Figure S14**, showing great similarity – which is an indication of well-built simulation model.

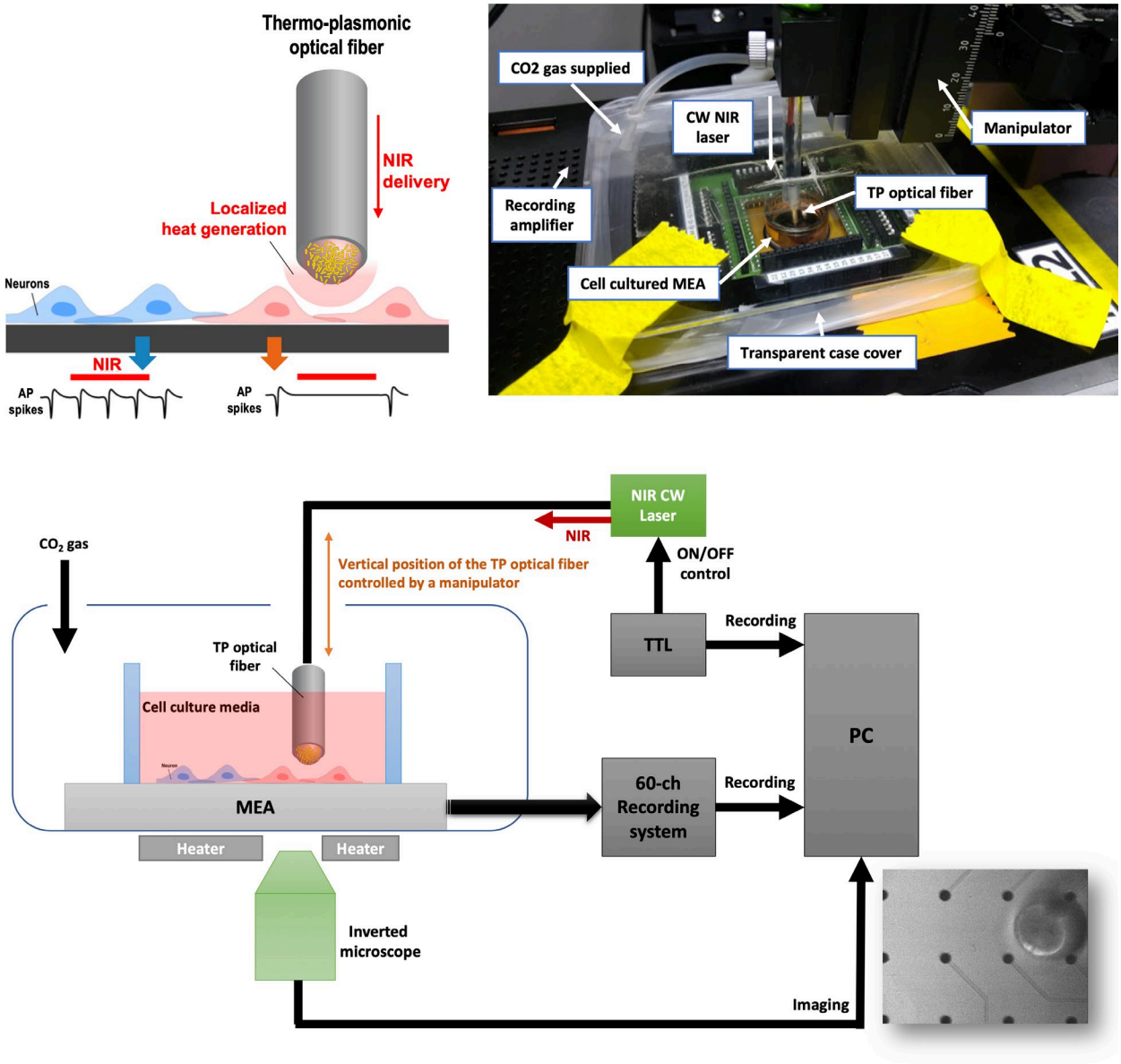

Figure S16. Photothermal neural stimulation experimental setup using the thermo-plasmonic optical fiber on the *in vitro* neuronal cell culture on microelectrode array chips. Illustration and pictures of the experimental setup. The MEA and its recording amplifier were placed on an inverted microscope.

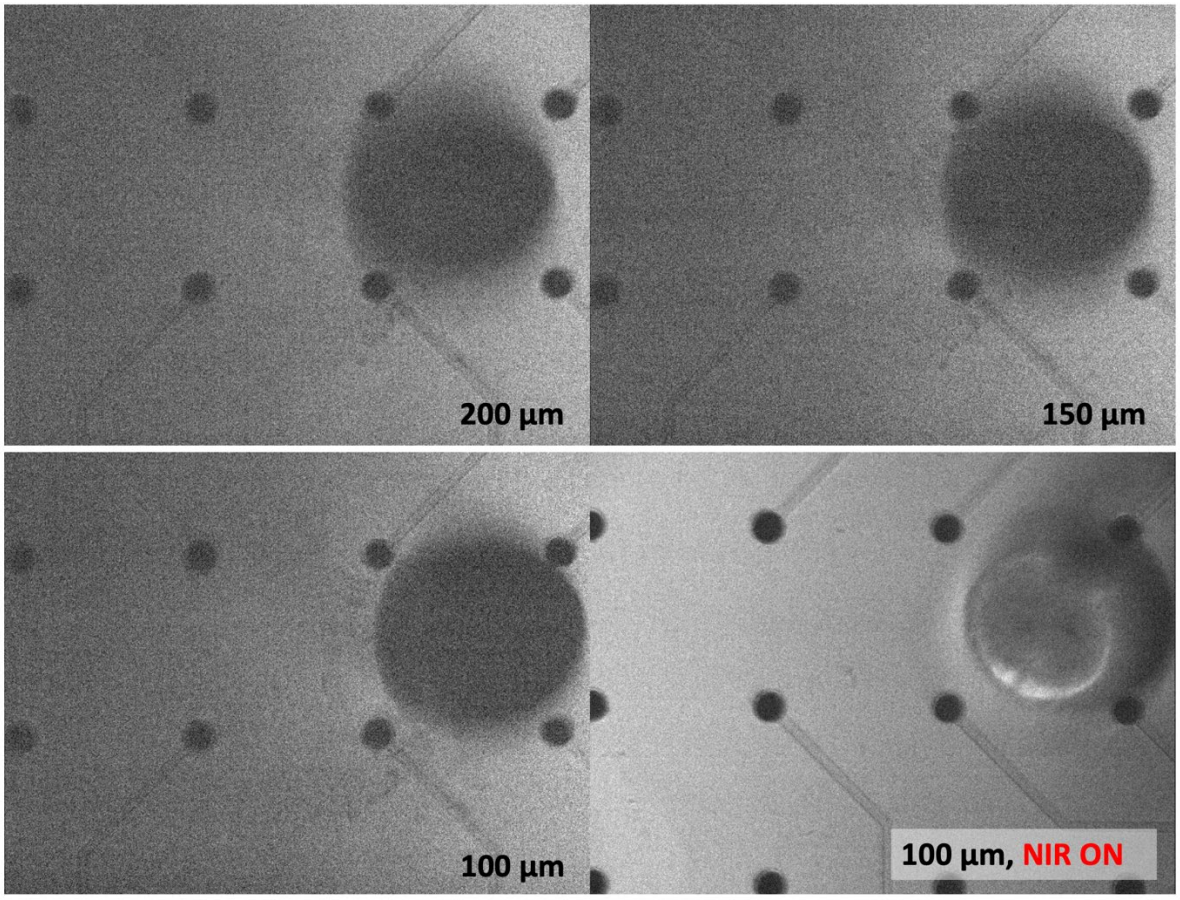

Figure S17. Inverted microscopic images of the optical fiber on an MEA chip with different distance between the optical fiber and the MEA chip. See the experimental setup in **Figure S16**. See the blurriness of the shadow of optical fiber changes with varying distance. The last photo is taken with the NIR laser turned on.

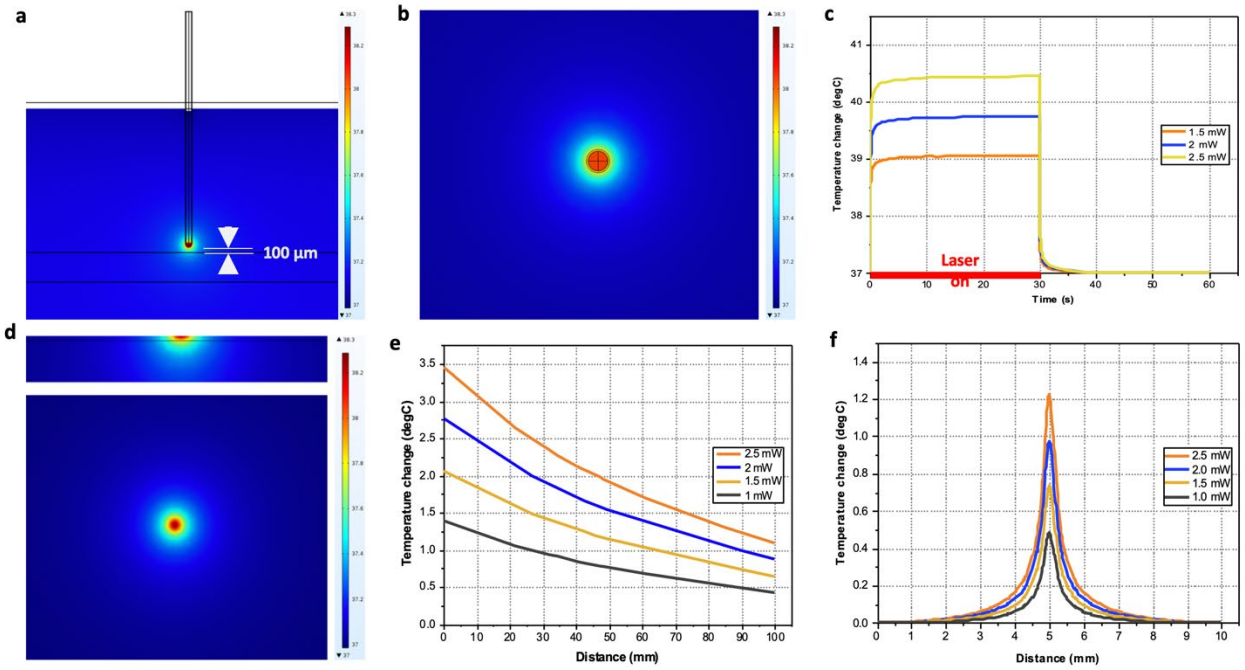

Figure S18. Computational thermal simulation of the optical fiber in water (*in vitro* neural stimulation environment). a, Side view of the temperature of optical fiber in water. Fiber to glass surface is defined as 100 µm. Applied input heat rate of 1 mW (equivalent to the light power of 6.74 mW). **b**, View from the bottom. Temperature of the surface of the thermo-plasmonic optical fiber. **c**, Peak temperature (center of the fiber) of the thermo-plasmonic optical fiber surface in **b** as the NIR laser turned on for 30sec and turned off immediately after that. Three different input heat rate conditions were simulated. **d**, Resultant temperature profile on the MEA quartz glass chip by the thermo-plasmonic effect form optical fiber. (Top) side view profile; (Bottom) Top view surface temperature profile. **e**, Attenuation of the thermo-plasmonic effect from the optical fiber through water. Distance in x-axis is defined as the distance (in µm) from the end of the DFL optical fiber. With respect to the distance, maximum temperature change from baseline temperature (*i.e.* 37 ºC) is plotted. Four different input heat rate in mW (1, 1.5, 2 and 2.5 mW; equivalent to 6.7, 10.1, 13.4 and 16.8 mW NIR laser power, respectively) were simulated. **f**, Lateral temperature profile (± 5 mm) from the center of the thermo-plasmonic optical fiber at peak temperature change. Four different input heat rate in mW (1, 1.5, 2 and 2.5 mW; equivalent to 6.7, 10.1, 13.4 and 16.8 mW NIR laser power, respectively) were simulated. Full width of half maximum (FWHM) of these plots are provided in the following **Table S1**.

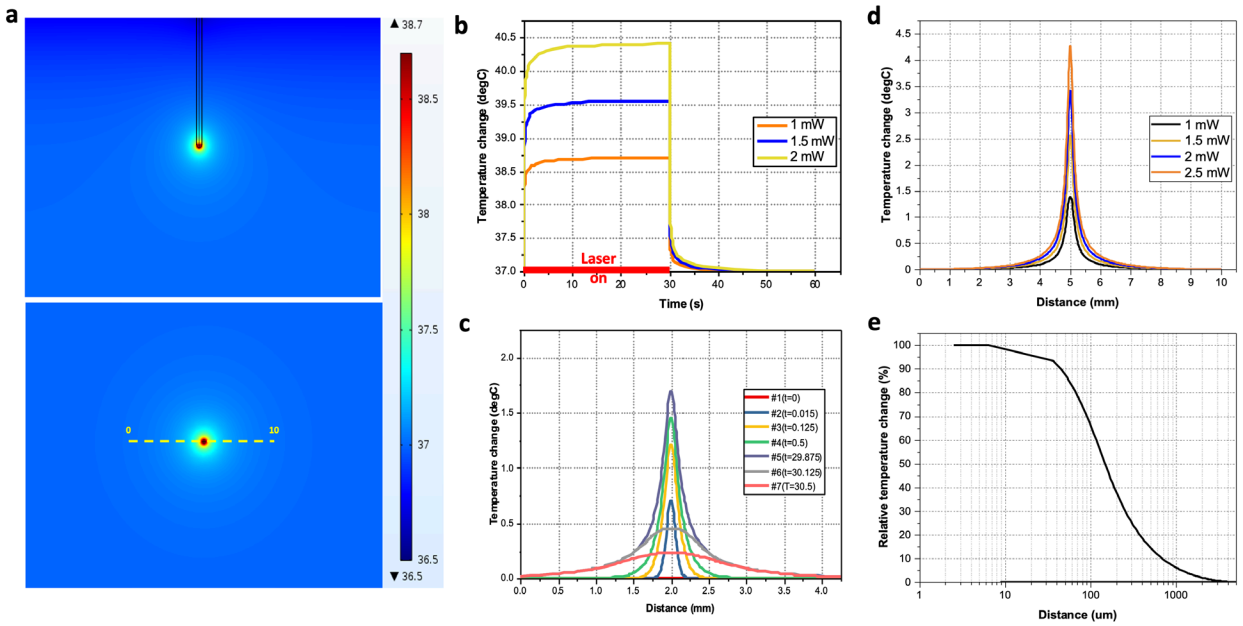

Figure S19. Computational thermal simulation of the optical fiber in brain (*in vivo* neural stimulation environment). a, Side view and bottom view of the temperature of TP optical fiber in brain. Applied input heat rate of 1 mW (equivalent to the light power of 6.74 mW). Temperature change profile is symmetric in any direction. **b**, Temperature of the tip of the thermo-plasmonic optical fiber. Peak temperature (center of the fiber) of the thermo-plasmonic optical fiber surface in **a** as the NIR laser turned on for 30sec and turned off immediately after that. **c**, Transient characteristics of the temperature change profile around the fiber when 1 mW of heat rate was applied. **d**, Lateral temperature profile (± 5 mm) from the center of the thermo-plasmonic optical fiber at peak temperature change. Four different input heat rate in mW (1, 1.5, 2 and 2.5 mW; equivalent to 6.7, 10.1, 13.4 and 16.8 mW NIR laser power, respectively) were simulated. **e**, Attenuation of the temperature change lateral direction described in **a**. 50% of attenuation from the center was observed at 145 μm, 75% at 300 μm, 90% at 662 μm.

Table S1. Full Width of Half Maximum (FWHM) of lateral temperature change from the thermo-plasmonic optical fiber in Figure S18f. Input heat rate conditions we simulated with are 1, 1.5, 2 and 2.5 mW (equivalent to 6.7, 10.1, 13.4 and 16.8 mW NIR laser power, respectively)

Heat rate (mW)	FWHM (μm)
1	535
1.5	538
2	540
2.5	540

a

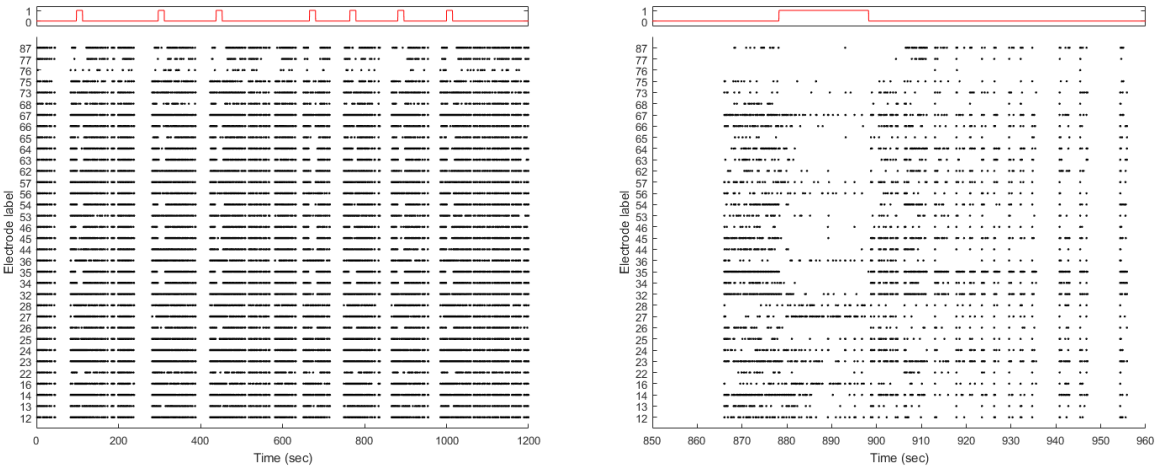

b

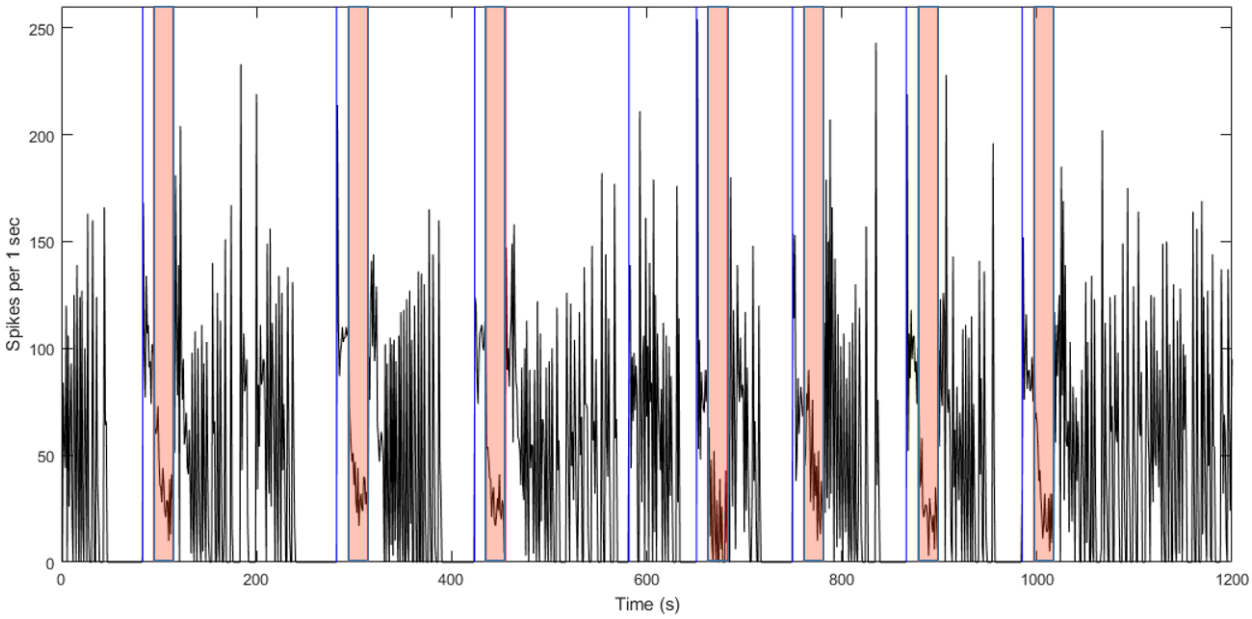

Figure S20. (MEA #2) a, Raster plots of electrical activity for active channels and photothermal stimulation timing used for the median burst delay calculation in **Figure 6**. **b,** Synchronized network burst activity used for the median burst delay calculation. The number of spikes in a bin size of 1 second is plotted over time. The spike count for each time is the sum of all active channels. The area colored with transparent red represents the point in time when a localized photothermal stimulation is applied on the channel 35. The blue line indicates that the group of successive spikes with short intervals are divided into long intervals.